Yttrium-modified Co3O4 as efficient catalysts for toluene and propane combustion: Effect of yttrium content

W. Zhang, C. Descorme, J. Luis Valverde, A. Giroir-Fendler

Yttrium-modified Co_3O_4 as efficient catalysts for toluene and propane combustion: Effect of yttrium content

Weidong Zhang,[†] *Claude Descorme,*[†] *Jose Luis Valverde,*[‡] *Anne Giroir-Fendler**[,†]

[†] Univ. Lyon, Université Claude Bernard Lyon 1, CNRS, IRCELYON, 2 Avenue Albert Einstein, Villeurbanne, F-69622, France

[‡] Department of Chemical Engineering, Faculty of Chemical Science and Technology, University of Castilla-La Mancha, Avenida Camilo José Cela 12, Ciudad Real, 13005, Spain

* Corresponding author: anne.giroir-fendler@ircelyon.univ-lyon1.fr

Abstract

A series of Y-modified cobalt oxides with various Y/(Co+Y) molar ratios (0.25%, 0.5%, 1%, 3% and 5%) were prepared to study the effect of Y content on toluene and propane combustion. The characterization of the catalysts revealed that proper Y incorporation resulted in smaller crystallite sizes, larger specific surface areas, more oxygen vacancies and weaker Co−O bonds. As such, the Y-modified Co_3O_4 showed enhanced low-temperature reducibility, boosted oxygen mobility and better catalytic activity. However, excess Y (> 1%) aggregates on the surface of Co_3O_4 and forms yttrium carbonate species, hindering the catalyst activity. A volcano-type relationship between the Y content and the catalytic activity was established. The optimal catalyst 1%Y-Co (with Y/(Co+Y) molar ratio of 1%) exhibited toluene oxidation rate of 24 nmol g^{-1} s^{-1} at 220 °C and propane oxidation rate of 69 nmol g^{-1} s^{-1} at 180 °C. Besides, 1%Y-Co presented perfect cycling stability and long-term durability in propane oxidation. Regarding its low cost, high efficiency and good stability, 1%Y-Co is a promising catalyst for the practical elimination of hydrocarbon emissions.

Keywords: Yttrium modification; Cobalt oxide; Oxygen mobility; Catalytic oxidation; Toluene; Propane

Environmental Implication

Hydrocarbon emissions including BTX (benzene, toluene, and o-xylene) and light alkanes have caused significant environmental and human health concerns. However, the elimination of such hazardous pollutants remains challenging. Catalytic oxidation is the most promising technique to address the problem. Herein, yttrium-modified Co_3O_4 catalysts were successfully designed for efficient destruction of toluene and propane at relatively low temperatures. The physicochemical properties characterizations reveal that an appropriate introduction of yttrium (1%) in Co_3O_4 could produce large surface area materials with enhanced redox ability. The present study provides a facile way to develop an inexpensive and high-performance catalyst for hydrocarbons elimination.

1. Introduction

Hydrocarbon emissions from a variety of sources, including fossil-fueled automobiles, petrochemical processes, industrial and power generation plants, and the treatment of solid and liquid wastes, contribute to a major group of atmospheric pollutants[1–3]. Among hydrocarbon exhausts, BTX (benzene, toluene and o-xylene), widely have high photochemical ozone creation potential [3] and high toxicity to human health [4,5]. On the other hand, light alkanes release has also drawn much attention because of i) the increase of light alkanes emitted from stationary sources as

55 the chemical processes and products develop [2,6,7], ii) the increasing utilization of
56 liquefied petroleum gas and compressed natural gas as substitutes for gasoline and
57 diesel vehicles [6,8], and iii) the difficulty to eliminate from engine exhaust emissions
58 due to their stable saturated C-H bond [9,10]. The control of BTX and light alkane
59 emissions is an essential and compelling issue. Catalytic oxidation is a promising
60 control technique characterized by its high efficiency, low operating temperatures and
61 low production of secondary pollutants. The key to this technique is the availability of
62 highly active, selective, and stable catalysts. In the past decades, transition metal
63 oxides have been extensively studied for hydrocarbon oxidation due to their lower
64 cost, higher thermal stability and better tolerability to poison compared with noble
65 metal catalysts. Co_3O_4 is an attractive transition metal oxide because it is not only one
66 of the most active catalysts for light alkanes combustion, with comparable
67 performance to some noble metal catalysts [11,12], but also exhibits excellent
68 performance for BTX removal [13–16].

69 To enhance the performance of Co_3O_4 catalysts, various routes have been
70 developed, e.g. nanocasting to obtain high-porosity Co_3O_4 [17], selectively exposing
71 the active crystal plane of Co_3O_4 [9], controlling the morphology of Co_3O_4 by
72 hydrothermal methods [14,15], treating Co_3O_4 with acid to create surface defects
73 [11,18], loading Co_3O_4 onto porous support to increase the dispersion of Co_3O_4
74 [19,20], forming composite oxide to have synergistic effects [2,8,21] and

75 incorporating a small content of other metals [22,23]. Wu et al. enhanced the activity
76 of Co_3O_4 for CO oxidation by replacing the Co^{2+} ions in the lattice with Cu^{2+} [24]. CO
77 oxidation activity of Co_3O_4 nanorods could also be elevated via the doping of V [23],
78 La [25] or Sn [26]. Baidya et al. prepared Fe- and Cr-doped Co_3O_4 catalysts by a
79 solution combustion technique and found a correlation between low-temperature CO
80 oxidation activity and the nature of the dopant [27]. Lee et al. found that Mn doping
81 into the (100) facets of Co_3O_4 cube could improve the activity of simultaneous
82 oxidation of CO, C_3H_6, and C_3H_8 [28]. Recently, our group demonstrated that the
83 propane oxidation activity over Co_3O_4 catalysts could be enhanced by a low doping
84 amount of Zr [29].

85 As an important material in the ceramic industry, yttria is usually used to prepare
86 well-known YSZ (yttria-stabilized zirconia) ceramics [30]. It is demonstrated that
87 anionic vacancies, which facilitate the accumulation and exchange of oxygen, can be
88 generated by the introduction of Y into zirconia [31]. Zanella et al. obtained
89 high-surface-area TiO_2 by Y doping and found that Y could restrain the growth of
90 TiO_2 crystal and stabilize the anatase structure [32]. Yang et al. reported that Y
91 doping led to smaller sizes of ZnO nanoparticles with better optical properties [33]. It
92 is interesting to choose Y as a modifier for Co_3O_4 based on the following reasons: i)
93 the larger ionic radius of Y than Co may induce distortion of structure and formation
94 of oxygen vacancies; ii) the lower electronegativity of Y than Co can lower the

95 d-band energy of Co to decrease the CO adsorption strength [34]; iii) the aggregated
96 Y_2O_3 can probably serve as pinning particles to inhibit the growth of Co_3O_4. It was
97 recently reported that the Y_2O_3 promoted Co_3O_4 catalyst showed excellent activity for
98 the catalytic decomposition of N_2O [35,36]. However, the co-precipitation method
99 used to synthesize the Y_2O_3-Co_3O_4 catalysts in these studies cannot achieve good
100 homogeneity of Y and Co, which limits the possible Y-Co interaction. To the best of
101 our knowledge, there are few publications concerning the synthesis of Y-modified
102 Co_3O_4 with high compositional homogeneity for catalytic combustion. Therefore, it is
103 highly desirable to prepare the homogeneous mutually dispersed Y-Co oxide catalysts
104 to maximize the redox properties of the catalysts.

105 Herein, we introduced Y to Co_3O_4 catalytic system by a facile citrate sol-gel
106 method with Y content ranging from 0 to 5%. The Y-modified Co_3O_4 catalysts were
107 systematically characterized using multiple techniques and evaluated for the total
108 oxidation of toluene and propane (representatives of BTX and light alkanes,
109 respectively). The objective of this work is to investigate the effect of Y content on
110 the structure and catalytic performance of cobalt oxide and to reveal the
111 structure-performance correlation.

2. Experimental

2.1. Catalyst preparation

Y-modified cobalt oxide catalysts were prepared via citrate sol-gel. The synthetic procedure is illustrated in **Fig. S1**. First, 5.821 g of $Co(NO_3)_2 \cdot 6H_2O$ (20 mmol; Alfa Aesar) and 0.019, 0.038, 0.077, 0.230, and 0.383 g of $Y(NO_3)_3 \cdot 6H_2O$ (0.05, 0.1, 0.2, 0.6, and 1 mmol; Aldrich Chemistry), together with 4.611 g of citric acid (24 mmol; Sigma-Aldrich) were dissolved and mixed in 50 mL of distilled water. Then, the mixed solution was evaporated at 80 °C under continuous water-bath stirring until a gel was formed. Next, the wet gel was foamed in an oven at 120 °C overnight. Finally, the obtained spongy solid was crushed into powder, calcinated in a furnace at 250 ℃ for 2 h and then 500 ℃ for 2 h at a heating rate of 2 °C min^{-1}. Samples with various Y/(Co+Y) molar ratios (0.25%, 0.5%, 1%, 3%, and 5%) were named as 0.25%Y-Co, 0.5%Y-Co, 1%Y-Co, 3%Y-Co, and 5%Y-Co, respectively. As controls, pure cobalt oxide (labeled Co) and yttrium oxide (labeled Y) were prepared by the same procedure.

2.2. Catalyst characterization

The as-prepared catalysts were characterized by various techniques including inductively coupled plasma-optical emission spectroscopy (ICP-OES), X-ray powder diffraction (XRD), Fourier transformed infrared (FTIR) spectroscopy, Raman spectroscopy, N_2 adsorption−desorption, Temperature-programmed reduction

experiments in hydrogen (H_2-TPR), thermal gravity-oxygen storage capacity (TG-OSC), and X-ray photoelectron spectroscopy (XPS). The details about the characterization methods are described in Section 1 of the Supporting Information.

2.3. Catalytic test

Catalytic tests were carried out in a U-shaped reactor (4 mm in internal diameter) using 0.15 g of the catalyst mixed with some silicon carbide (~ 0.55 g) to avoid hot spots. The reaction temperature was measured by a K-type thermocouple inserted into the catalytic bed. The total flow rate was kept at 100 mL min^{-1}, giving a weight hourly space velocity (WHSV) of 40,000 mL g^{-1} h^{-1}. Detailed test conditions of toluene and propane oxidation are provided in Section 2 of the Supporting Information.

3. Results and discussion

3.1. Decomposition of the precursors

Fig. S2 shows the FTIR spectra of pure Co, 1%Y-Co, and 5%Y-Co foaming precursors. There is no obvious difference among the spectra. The broad band between 2800−3600 cm^{-1} indicated the presence of adsorbed H_2O and O−H group [37]. The bands at 845 and 1385 cm^{-1} were attributed to the nitrate species [37]. The bands at ca. 1575 and 1395 cm^{-1} were from the asymmetric and symmetric stretching vibrations of COO^- [37], and the bands at ca. 620 and 550 cm^{-1} from vibrations of Co−O [38]. The FTIR spectra of the precursors are consistent with the characteristics

of mixed metal citrate complexes. Homogeneously mixed-metal citrate complexes formed due to the three-ligand nature of citrate, which ensures the homogeneity of the Y-Co precursors.

The thermal decomposition process of the catalyst precursors has been investigated by TG/DTA (**Fig. S3**). From room temperature to 120 °C, only slight weight loss was observed due to the evaporation of adsorbed H_2O. From 120 °C to 360 °C, significant weight loss ascribed to the decomposition of cobalt citrates and nitrates was observed, accompanied by a large exothermic peak at around 330 °C in the DTA profile. Further increasing the temperature to 625 °C caused imperceptible weight loss, suggesting the completion of the whole reaction and the stability of the final product.

3.2. Structural and textural properties

The weight percentages of Co and Y in the catalysts were determined by ICP-OES (**Table 1**). The calculated Y/(Co+Y) atomic ratios were basically consistent with the nominal ones. The structure and crystallinity of the catalysts were investigated by XRD (**Fig. 1**). The Y sample exhibited typical diffraction peaks of cubic Y_2O_3 crystal (JCPDS PDF# 71-0049, a = 10.596 Å), while the diffraction peaks of Co and Y-Co oxides can be well indexed to cubic spinel Co_3O_4 phase (JCPDS PDF# 74-2120, a = 8.0840 Å) with Fd3m (227) space group. For all Y-Co oxides, no diffraction peaks corresponding to Y_2O_3 phase were observed, suggesting that the yttrium species may be incorporated into the Co_3O_4 crystal lattices, uniformly distributed in the Co_3O_4

matrix, or highly dispersed on the surface of cobalt oxide in an amorphous state. As the Y content increases from 0 to 5%, the diffraction peaks of Y-Co oxides get weaker and broader, indicating a declined crystallinity and a smaller crystallite size. Additionally, the peaks corresponding to the (311) plane of Co_3O_4 in the Y-Co oxides shifted to a lower angle compared with that of pure cobalt oxide. The average crystallite size (d) and lattice constant (a) of these oxides were estimated by the MDI Jade 6.0 program (**Table 1**). With increasing Y content, the crystallite size decreased. Regarding the lattice constant, the Y-Co oxides exhibited larger values than pure Co_3O_4, while no significant difference was observed when the Y concentration increased. A possible explanation is that only a bit of Y ions could enter the Co_3O_4 lattice, causing lattice expansion and defects; excessive Y_2O_3 might highly disperse in the matrix or on the surface of Co_3O_4. Since Y^{3+} (0.104 Å) has a larger ionic radius than Co^{3+} (0.685 and 0.75 Å in low and high spin state, respectively) or Co^{2+} (0.79 and 0.885 Å in low and high spin state, respectively), it was likely to locate at the interface, crystal boundary of Co_3O_4, or serve as pinning particles, and thereby restraining the nucleation and growth rate of Co_3O_4 during the calcination process [23,39].

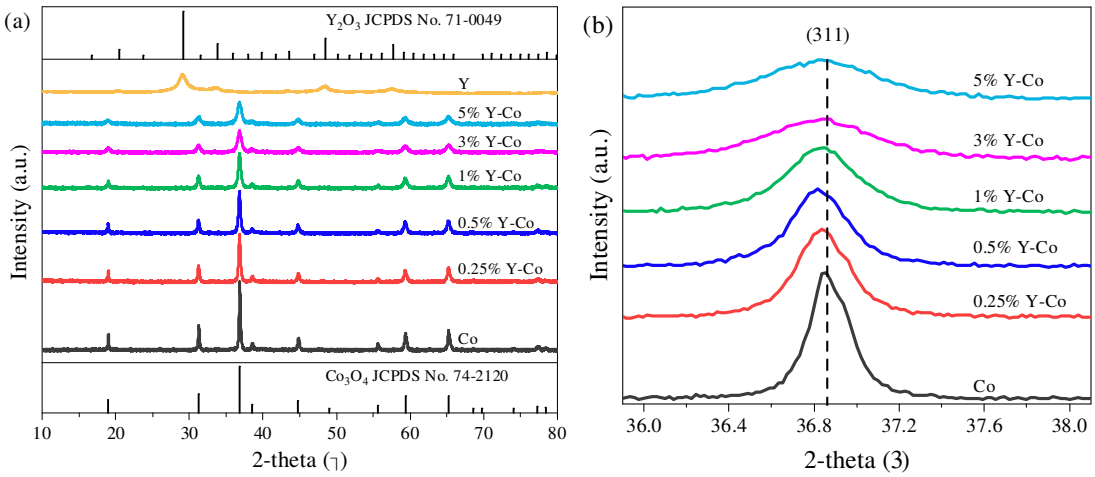

189

190 **Fig. 1.** (a) XRD patterns of the catalysts and (b) diffraction peaks of the (311) crystal

191 plane.

192 **Table 1.** The physicochemical properties of the catalysts.

Catalysts	Y/Co [a] (wt.%)	Y/(Co+Y) [a] (at.%)	d [b] (nm)	a [b] (Å)	SSA [c] (m^2 g^{-1})	V_{pore} [c] (cm^3 g^{-1})
Co	0/73.3	0	58	8.085	6	0.02
0.25%Y-Co	0.3/72.7	0.27	36	8.092	10	0.06
0.5%Y-Co	0.6/73.2	0.54	31	8.094	18	0.08
1%Y-Co	1.1/72.0	1.00	24	8.093	30	0.13
3%Y-Co	3.3/69.2	3.06	14	8.093	47	0.14
5%Y-Co	5.4/67.0	5.07	13	8.093	55	0.17
Y	77.5/0	100	6	10.626	25	0.06

[a] Determined and calculated by ICP analysis; [b] average crystallite size and lattice constant from XRD patterns; [c] specific surface area and total pore volume determined by N_2 adsorption.

Fig. 2 depicts the FTIR spectra of the oxides. Looking at pure Co oxide, two intense bands were observed at around 654 and 539 cm^{-1}, corresponding to the stretching vibration of tetrahedrally coordinated Co^{2+}–O and octahedrally coordinated Co^{3+}–O, respectively [40]. For pure Y oxide, the two bands at ~557 and 459 cm^{-1} are attributed to the Y–O vibration of cubic Y_2O_3 [41]. Additionally, the intense double peaks at 1504 and 1411 cm^{-1} correspond to υ3 mode of CO_3^{2-}, whereas the bands at ~1075 and 845 cm^{-1} correspond to υ1 and υ2 modes of CO_3^{2-}, respectively [42]. The abundant presence of carbonate species suggests that Y_2O_3 can react with CO_2 in air to form $Y_2(CO_3)_3$ or $YOHCO_3$. Regarding Y-Co oxides, the characteristic bands of Co_3O_4 were well maintained, in agreement with XRD analysis. Interestingly, some new bands corresponding to carbonate species were clearly observed in 3% and 5%Y-Co. Considering that no carbonate species were identified for pure Co_3O_4, we deduced that at low content, Y^{3+} is randomly dispersed throughout the Co_3O_4 particle, whereas large Y_2O_3 particles aggregate on the surface of Y-Co oxide when Y/(Co+Y) > 1%.

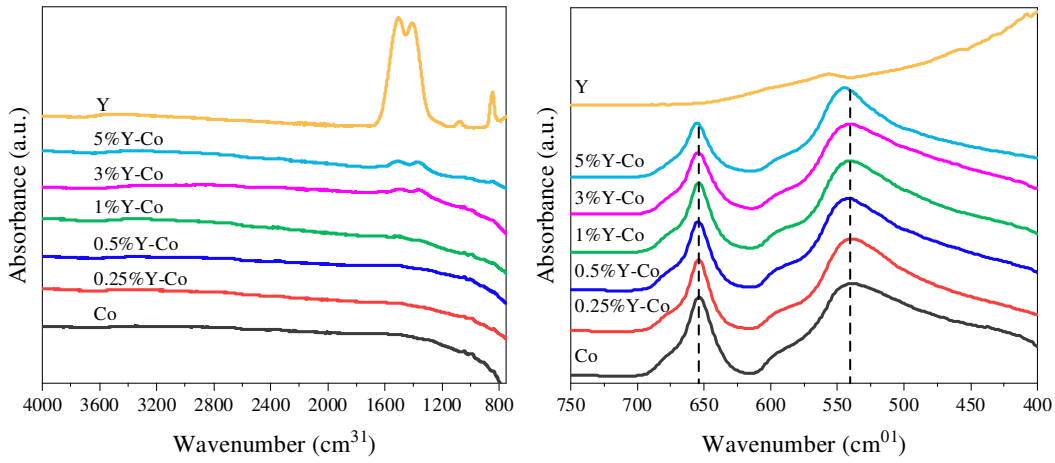

Fig. 2. FTIR spectra of the catalysts.

To further study the effect of Y content on the Co_3O_4 structure and unravel the formation of defects, Raman spectra were collected (**Fig. 3a**). For pure Co oxide, five characteristic peaks corresponding to the stretching mode of spinel Co_3O_4 were clearly observed [11,43,44], which agrees well with the XRD and FTIR analyses. The peak at 676 cm^{-1} was assigned to the octahedral sites (CoO_6) with A_{1g} symmetry. The weak peak at 605 cm^{-1} was due to the F^3_{2g} symmetry. The two medium-intensity peaks centered at around 507 and 467 cm^{-1} were associated with the F^2_{2g} and E_g symmetry modes, respectively. The peak at 180 cm^{-1} was attributed to the tetrahedral sites (CoO_4) with F^1_{2g} symmetry. Compared with pure Co oxide, the Raman peaks of Y-Co oxides weakened and broadened with increasing Y/(Co+Y) ratios, indicating the formation of lattice defects and oxygen vacancies, which induced weaker Co–O bonds of the catalyst [45,46]. The Co–O bond force constant (k), reflecting the Co–O bond strength, was estimated based on the Raman shift of A_{1g} mode according to Hooke's law [13,46,47]. As shown in **Fig. 3b**, the k value of the catalysts gradually

decreased with the increase of Y content, demonstrating that Y modification weakened the Co–O bond in Co_3O_4. The presence of oxygen vacancies could enhance the electron density of their surrounding lattice oxygen, decrease the binding energy of lattice oxygen and thus weaken the Co–O bond [46]. According to Ref [34], the surface concentration of Co^{2+} and Co^{3+} is proportional to the areal intensity ratio of F^1_{2g} and A_{1g}. By integration, these values were estimated and listed in **Table 2**. It can be seen that Y introduction led to higher F^1_{2g}/A_{1g} ratio, which could be related to the formation of oxygen vacancies [43]. Among the Y-Co oxides, 1%Y-Co exhibited the largest amount of oxygen vacancies.

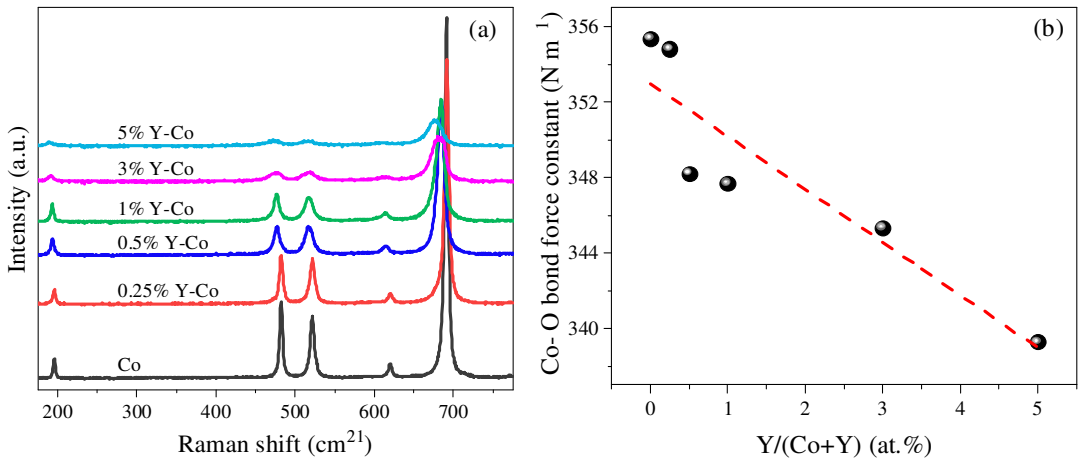

Fig. 3. (a) Raman spectra of the catalysts and (b) Correlation between the Co–O bond strength and the Y/(Co+Y) atomic ratios.

Table 2. Quantitative analysis of Raman spectra, H_2-TPR and TG-OSC, and O_2-TPD profiles of the catalysts.

Catalysts	Raman	H_2 uptake (mmol	TG-OSC (%)	O_2 desorption

	spectra	g^{-1})				(μmol g^{-1})	
	Areal ratios of F^1_{2g}/A_{1g}	50–300°C	Total	O_α	O_β	O_α	O_β
Co	0.023	1.5	16.5	0.01	-0.11	0.54	3.99
0.25%Y-Co	0.025	1.8	15.4	0.09	-0.02	0.69	4.14
0.5%Y-Co	0.036	1.9	15.1	0.16	0.08	1.02	5.42
1%Y-Co	0.040	2.3	14.9	0.37	0.29	1.62	7.46
3%Y-Co	0.037	1.6	12.6	0.69	0.64	1.44	13.1
5%Y-Co	0.036	1.2	11.9	1.02	1.02	1.16	19.2

Fig. 4 shows N_2 adsorption-desorption isotherms and BJH pore size distributions of the oxides. The specific surface area (SSA), pore volume (V_{pore}), and average pore size (D_{pore}) are summarized in **Table 1**. According to the IUPAC classification, all Y-Co oxides exhibited Type IV isotherm curves with H1-shaped hysteresis loops, indicating the presence of mesopores. Pure Co oxide is almost non-porous with a low SSA of 6 m^2 g^{-1}. The introduction of Y increased the porosities of the Y-Co oxides; the more Y added, the larger SSA and V_{pore} were obtained, which agrees well with the decrease in crystallite size. Y modification also affected the pore size of the Y-Co oxides. The average pore size decreased from 25 nm to 10 nm as the Y amount increased from 0.25% to 5%, meanwhile, the pore size distribution became more and more centralized. The large surface area and pore volume could facilitate mass

transfer and the adsorption of reactants, while the small pore size might facilitate the full contact between the reactants and the catalyst by extending the residence time of reactants [35], which benefits the catalytic combustion.

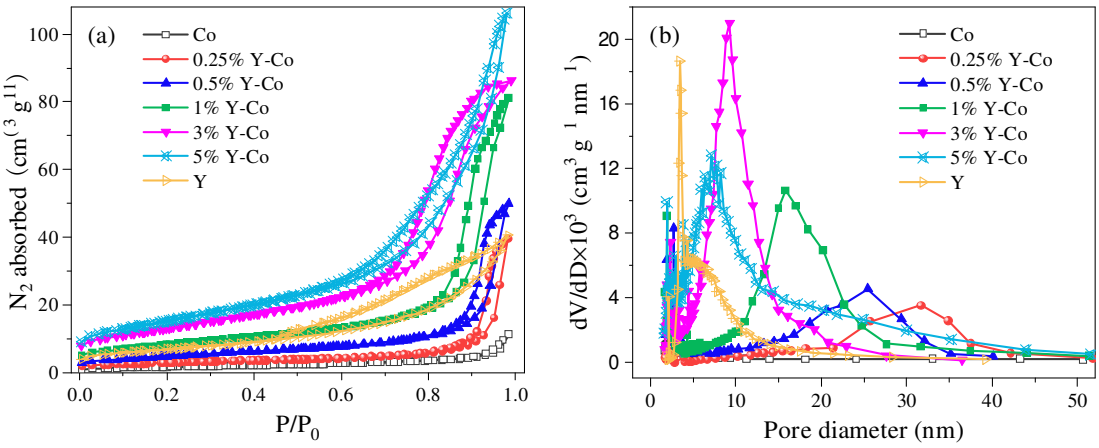

Fig. 4. (a) N_2 adsorption-desorption isotherms and (b) BJH pore size distributions of the catalysts.

3.3. Redox ability

It is well-accepted that the catalytic oxidation of hydrocarbons over transition metal oxides proceeds via a redox mechanism [48], in which the redox ability of the catalyst plays a crucial role.

H_2-TPR experiments were conducted to study the effect of Y modification on the reduction behavior of Co_3O_4. The results are shown in **Fig. 5a**. Pure Y_2O_3 exhibits no appreciable reduction peak, indicating Y_2O_3 is irreducible within the test temperature range. For pure Co_3O_4, a broad peak was observed, which was due to the overlapping of two peaks corresponding to the stepwise reduction of Co^{3+} to Co^{2+} and Co^{2+} to Co^0.

In terms of Y-Co oxides, these two reduction peaks could be clearly identified. As Y content increased from 0% to 1%, the low-temperature reduction peak shifted to lower temperature, suggesting the enhanced low-temperature reducibility caused by Y-Co interaction and size effect [49], whereas the high-temperature reduction peak remained unchanged. Further increase in Y content to 3% or 5% resulted in worse reducibility, reflected by the significant shift of both two reduction peaks to higher temperatures. As evidenced by FTIR analysis, excessive Y_2O_3 can aggregate on the surface of the Y-Co oxides, which may hinder the reduction of Co_3O_4.

The total H_2 uptake amount of pure Co oxide was 16.5 mmol g^{-1} (**Table 2**), which is identical to that of the stoichiometric Co_3O_4 (16.6 mmol g^{-1}). This value decreased with increasing Y content due to the irreducible nature of Y_2O_3. To better compare the low-temperature reducibility of these catalysts, the H_2 uptake amount between 50 °C and 300 °C was quantified (**Table 2**). It is clear that more H_2 was consumed by 1%Y-Co up to 300 °C than other catalysts. Moreover, the initial H_2 consumption rate, which is frequently used to evaluate the low-temperature reducibility of oxide catalysts [9,50], was also calculated based on the H_2 consumption per gram of catalyst per second (**Fig. 5b**). Evidently, the initial H_2 consumption rate varied as follows: 1%Y-Co > 0.5%Y-Co > 0.25%Y-Co > 3%Y-Co ≈ Co > 5%Y-Co.

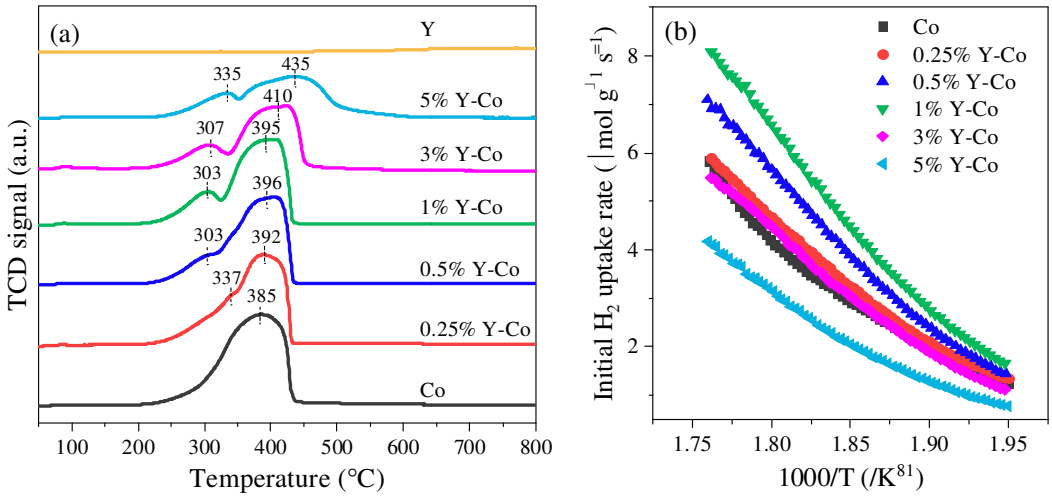

286

287 **Fig. 5.** (a) H_2-TPR profiles and (b) initial H_2 consumption rate curves of the catalysts.

288 To get insight into the oxygen storage and release capacity of the oxides, TG
289 experiments under N_2 were carried out after pretreating the oxides by air. **Fig. 6a**
290 shows the TG weight loss curves from 25 to 800 °C. For all catalysts, the weight loss
291 below 100 °C corresponded to the removal of physically adsorbed oxygen. In the
292 range of 100–700 °C, the weight loss was divided into two regions: the one below 300
293 °C is ascribed to the removal of surface chemisorbed oxygen species (O_α), whereas
294 the latter was associated with the depletion of surface lattice oxygen species (O_β). The
295 large weight loss detected above 700 °C is due to the conversion of Co_3O_4 to CoO. As
296 listed in **Table 2**, the released amount of either α or β oxygen increased with Y
297 concentration. This indicates that the introduction of Y can facilitate the formation of
298 oxygen vacancies and enhance the oxygen mobility of Co_3O_4. However, it should be
299 pointed out that some Y carbonate species may be present in 3%Y-Co and 5%Y-Co,
300 which can also cause a weight loss in the TG-OSC curves. O_2-TPD experiments were

further performed to study various types of oxygen species over the catalysts (**Fig. 6b**). Three types of oxygen desorption peaks were observed in the temperature range of 50–300 °C, 300–650 °C and 650–850 °C, which correspond to adsorbed oxygen species (O_α), surface lattice oxygen (O_β) and bulk lattice oxygen, respectively [16]. The quantified amount of desorbed O_α and O_β is given in Table 2. The desorption amount of O_α species follows the order of 1%Y-Co > 3%Y-Co > 5%Y-Co > 0.5%Y-Co > 0.25%Y-Co > Co. Interestingly, 1%Y-Co desorbed more adsorbed oxygen species than other catalysts, suggesting the presence of higher quantities of oxygen vacancies in 1%Y-Co, which agrees well with the Raman analyses. The desorbed O_β species increased with increasing Y content, which is consistent with the TG-OSC results.

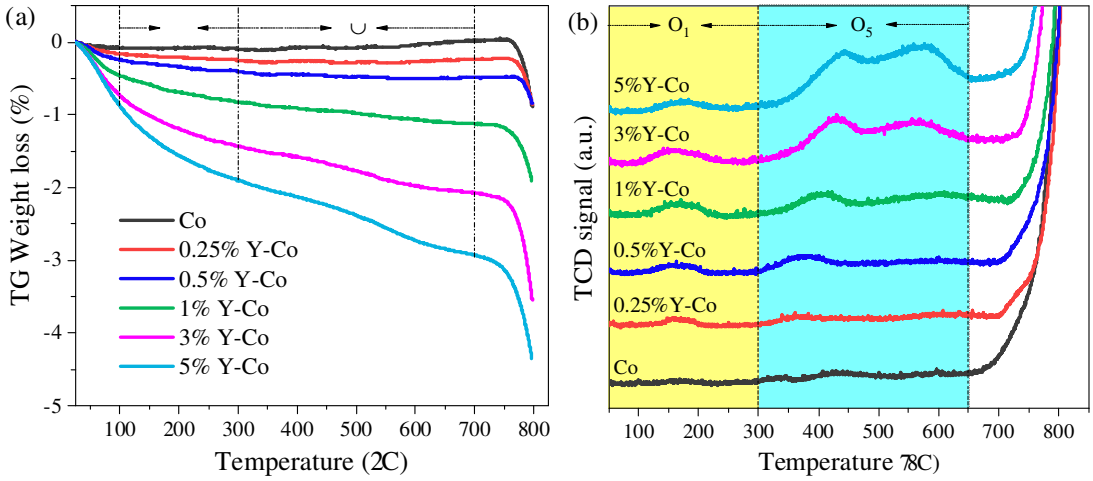

Fig. 6. (a) TG-OSC and (b) O_2-TPD profiles of the catalysts.

3.4. Surface species

The catalytic activity of the oxides is closely related to their surface physicochemical properties. To investigate the effect of Y content on the surface chemical compositions and surface oxygen species, XPS spectra were recorded. As illustrated in **Fig. S4a**, the XPS survey spectra revealed the presence of Co, O and Y elements in Y-Co samples. The surface atomic ratio of each element obtained by integration is summarized in **Table 3**. The results suggested a slight enrichment of Y on the surface of Y-Co samples. The detailed photoemission peaks of Y 3d are shown in **Fig. S4b**. The peak intensity of Y 3d increased with increasing Y content in the Y-Co samples. The peaks of Y $3d_{5/2}$ in Y-Co samples occurred at 157.2 eV, showing a shift of 0.6 eV compared with that (156.6 eV) in Y_2O_3 nanocrystals [51], which may be associated with either oxygen trapping or the existence of Y carbonate species. It was reported that Y_2O_3 tends to adsorb CO_2 from the atmosphere to form carbonate species [52,53], which was also supported by the FTIR analysis. The presence of carbonate species was further confirmed by the peaks at ~288.4 eV occurred in the C 1s spectra (**Fig. S4c**). **Fig. 7** presents the Co 2p and O 1s XPS spectra of the oxides. The main peak positions of the Co 2p doublet ($2p_{1/2}$ and $2p_{3/2}$) are at ~ 794.7 and 779.7 with a spin-orbit splitting of ~ 15.0 eV, along with two weak satellite peaks, similar to those reported for pure Co_3O_4 [2,14,17]. According to some literature [2,14,17], the Co $2p_{3/2}$ spectra were deconvoluted into two components peaks, one for Co^{2+} (ca. 781.5 eV) and the other for Co^{3+} (ca. 779.7 eV). As shown in **Table 3**, the

surface Co^{2+}/Co^{3+} atomic ratio first increased and then decreased with Y content. 1%Y-Co exhibited the highest concentration of surface Co^{2+}, indicating the presence of abundant oxygen vacancies, which is in line with the Raman analysis. The O 1s spectra were decomposed into two peaks. The one at 531.2 eV was associated with the surface adsorbed oxygen species (O_{ads}) while the one at ca. 529.3 eV was assigned to surface lattice oxygen (O_{latt}) [54,55]. With the increase of Y concentration from 0 to 5%, the O_{ads}/O_{latt} value increased progressively. However, as mentioned above, the Y carbonates species present on the surfaces of 3%Y-Co and 5%Y-Co can also contribute to the O_{ads} value due to their similar binding energy position and thus could cause an overestimation of the amount of O_{ads} in 3%Y-Co and 5%Y-Co. Summarizing up, 1%Y addition in Co_3O_4 favored the formation of surface oxygen vacancies and adsorbed oxygen species, which can participate in hydrocarbons oxidation.

Table 3. XPS characteristics of the catalysts.

Catalysts	Surface concentration (at.%)			Surface molar ratio	
	Y	Co	O	Co^{2+}/Co^{3+}	O_{ads}/O_{latt}
Co	0	32.5	57.4	0.39	0.41
0.25%Y-Co	0.4	31.4	57.1	0.42	0.58
0.5%Y-Co	1.1	30.9	57.0	0.46	0.63
1%Y-Co	1.7	28.4	56.8	0.57	1.13
3%Y-Co	3.9	27.5	55.5	0.41	2.70

5%Y-Co	6.1	26.1	53.8	0.39	2.89

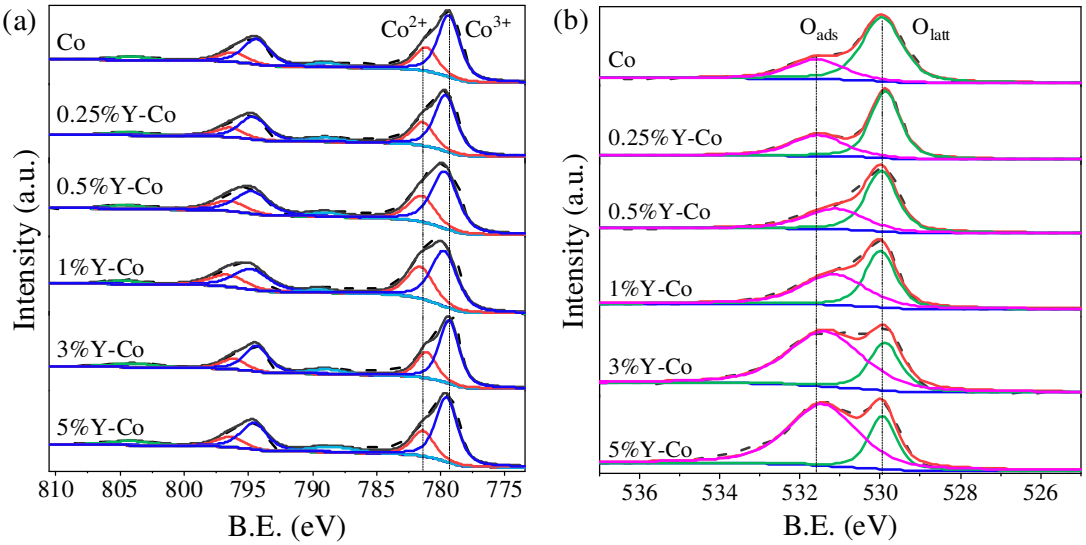

Fig. 7. (a) Co 2p and (b) O 1s XPS spectra of the catalysts.

3.5. Catalytic performance

All catalysts were tested in the total oxidation of toluene and propane for one heating–cooling catalytic cycle. To avoid overestimation of mineralization rate due to adsorption or incomplete conversion of hydrocarbon, CO_2 yield instead of hydrocarbon conversion was used in the light-off curves. Because of the accumulation of intermediates and excessive release of CO_2 during the heating process of toluene oxidation (**Fig. S5a and S6b**), the light-off curves obtained upon the cooling stage were applied to compare the catalytic performance. **Fig. 8** shows the catalytic performance of the prepared catalysts for toluene or propane oxidation under oxygen-rich conditions. T_{10}, T_{50} and T_{90} values (temperatures at 10, 50 and 90% toluene or propane conversion, respectively) were summarized in **Table S1** and **S2**.

In toluene oxidation, pure Y_2O_3 was almost inert, with only 2% toluene converted at 350 ºC, whereas pure Co_3O_4 exhibited good performance (T_{90} = 291 ºC). Benefiting from the introduction of Y species, the catalytic performance of pure Co_3O_4 was greatly enhanced, evidenced by the shift of light-off curves towards lower temperature range. The best performance was achieved when the Y/(Co+Y) ratio reached 1%. The T_{50} value of catalyst 1%Y-Co (244 ºC) was 31 ºC lower than that of pure Co_3O_4 (275 ºC). Further increasing of the Y content in Y-Co catalysts inhibited their activity at the high-temperature stage, though their low-temperature performance could be further improved. The produced CO and CO_2 during the toluene oxidation process were in situ monitored and displayed in **Fig. S6**. As a function of Y content in Co_3O_4, the concentration of by-product CO had an obvious tendency of dropping while the bump in the CO_2 evolution curve caused by the sudden decomposition of accumulated intermediate of toluene oxidation got bigger. Therefore, the incorporation of Y in Co_3O_4 could inhibit the production of CO during toluene combustion.

Regarding the propane oxidation, pure Y_2O_3 presented poor performance again (1.6% of propane conversion at 350 ºC). However, the effect of Y modification on propane oxidation was a bit different from that on toluene oxidation. The catalytic performance of Y-Co catalysts increases with Y content up to a Y concentration of 1% and then decreased gradually. The T_{90} value of 1%Y-Co (242 ºC) was 27 ºC lower than that of pure Co_3O_4, while the T_{90} value of 5%Y-Co (323 ºC) was 54 ºC

higher than that of pure Co_3O_4. Thus, a low content of Y modification can improve the activity of Co_3O_4 in propane oxidation, whereas superfluous Y addition to Co_3O_4 could be detrimental to propane oxidation, especially in the high-temperature range. During the catalytic reactions, only trace amounts of propene were produced (**Fig. S7**), indicating the excellent selectivity of the prepared catalysts for propane oxidation.

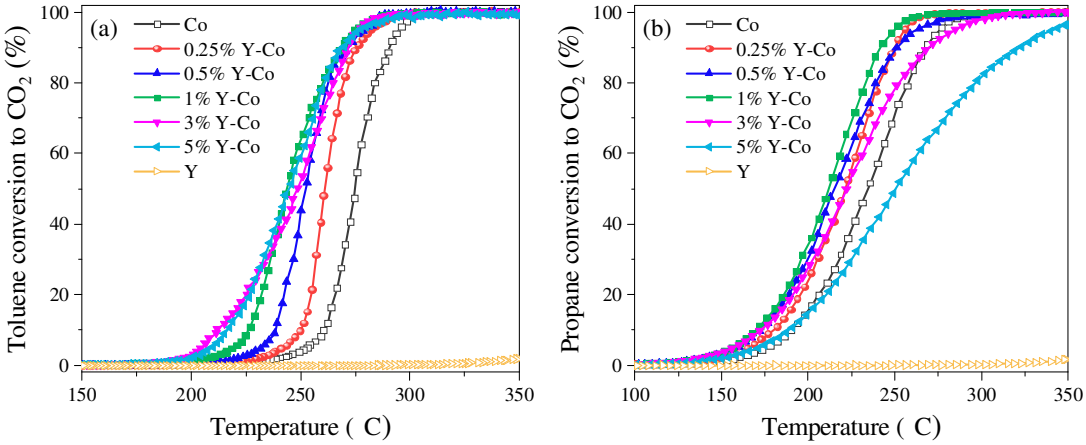

Fig. 8. (a) Toluene and (b) propane conversion to CO_2 as a function of temperature over the catalysts (reaction conditions: toluene/propane concentration = 1000 ppm, O_2 concentration = 21 vol.% and WHSV = 40,000 mL g^{-1} h^{-1}).

By assuming that toluene and propane oxidation under the oxygen-rich atmosphere follows the first-order reaction kinetics model, the Arrhenius curves of –ln r vs 1000/RT for all catalysts were plotted in **Fig. S8** (the corresponding reactant conversions were 1–8%). As summarized in **Table S1** and **S2**, for toluene oxidation, 1%Y-Co catalyst exhibited the lowest apparent activation energy and pre-exponential

397 factor. For propane oxidation, the E_a values decreased with an increase of Y content,
398 as the ln A values do. **Fig. S9** revealed a compensation effect between the E_a and lnA
399 values [56].

400 The reaction rates and specific reaction rates of the catalysts were calculated and
401 listed in **Table S1** and **Table S2**. For both toluene and propane oxidation, the
402 Y-modified Co3O4 catalysts exhibited higher reaction rates than pure Co_3O_4.
403 However, regarding the specific reaction rates, the values of the Y-modified Co_3O_4
404 catalysts were larger than that of pure Co_3O_4 in toluene oxidation while the value of
405 pure Co_3O_4 was the largest in propane oxidation. This phenomenon suggests that the
406 large specific surface areas of the Y-Co catalysts contributed a lot to their enhanced
407 propane oxidation performance, whereas the enhanced toluene oxidation performance
408 of the Y-Co catalysts was mainly due to their increased intrinsic activity. Combining
409 the catalytic activity in both toluene and propane oxidation, 1%Y-Co was considered
410 the optimal catalyst. As shown in **Table S3**, the catalytic performance of catalyst
411 1%Y-Co in toluene and propane combustion was comparable to or even better than
412 most catalysts recently reported in the literature. Considering the simple preparation
413 method and low cost, 1%Y-Co can be a candidate for the practical elimination of
414 hydrocarbon emissions. The cycling stability and long-term durability of 1%Y-Co
415 were investigated. As shown in **Fig. 9a and 9b**, 1%Y-Co exhibited excellent cycling
416 stability, as evidenced by the identical light-off curves upon three consecutive

catalytic cycles in both toluene and propane oxidation processes. As shown in **Fig. 9d**, 1%Y-Co exhibited outstanding long-term performance in propane oxidation, almost no deactivation was observed after a 29-h continuous test at either 239 ℃ or 194 ℃. However, significant activity loss occurred for 1%Y-Co in long-term toluene oxidation (**Fig. 9c**). This can be explained by the accumulation of intermediate on the surface of the catalyst, considering excess amount of CO_2 was produced during the heating reaction cycle in the high-temperature region (**Fig. S5a and S6b**). Nevertheless, this kind of deactivation is reversible. When the catalyst was treated in air for a while, the carbonate species deposited on the surface of the catalyst can be quickly burned out and consequently the catalyst was completely regenerated. The reversible inactivation in toluene oxidation but stable performance in propane oxidation of the Y-Co catalysts were further confirmed by performing the long-term test over 0.5%Y-Co (**Fig. S10**).

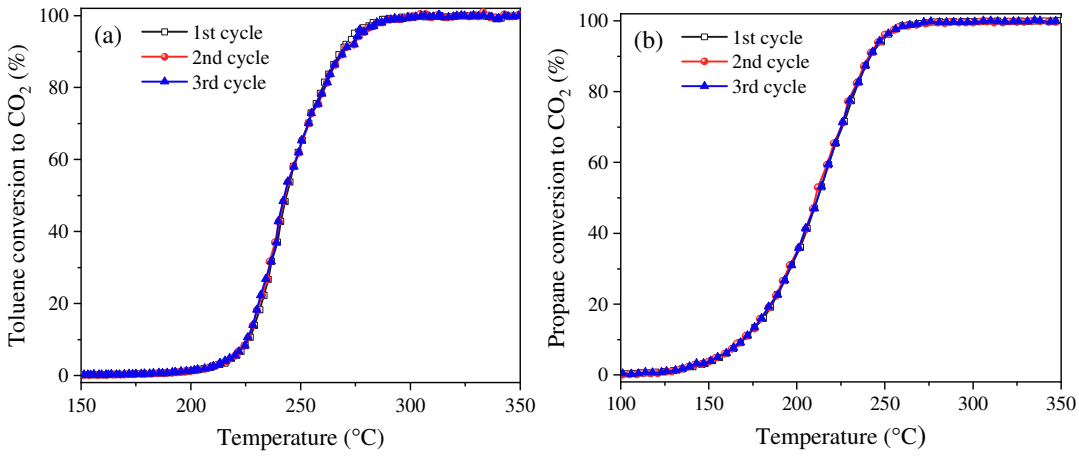

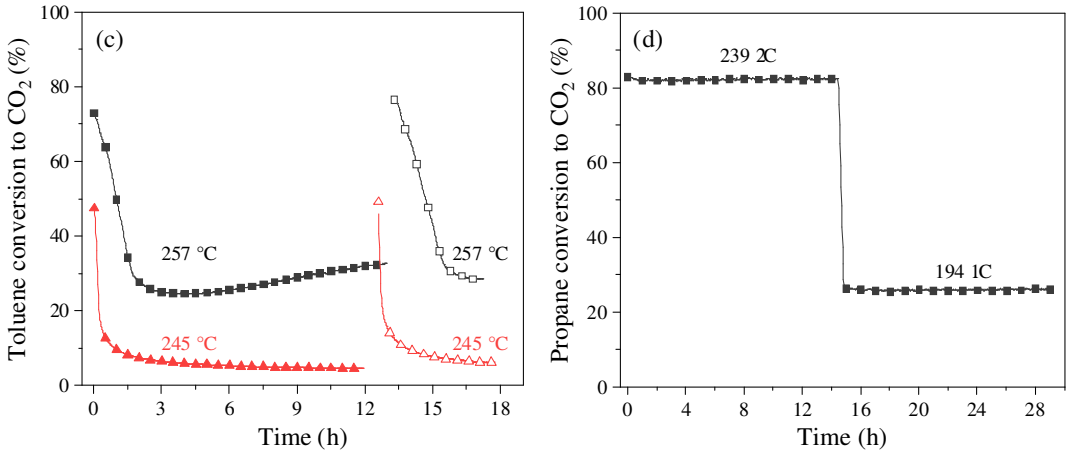

Fig. 9. (a) Toluene and (b) propane conversion to CO_2 as a function of temperature over 1%Y-Co upon three consecutive catalytic cycles; (c) Toluene and (d) propane conversion to CO_2 as a function of time on stream over 1%Y-Co (reaction conditions: toluene/propane concentration = 1000 ppm, O_2 concentration = 21 vol.% and WHSV = 40,000 mL g^{-1} h^{-1}).

In practical applications, water vapor is widely present and thus the effect of 5 vol.% H_2O on the catalytic oxidation of propane over typical catalysts was studied (**Fig. 10**). Introduction of 5 vol.% H_2O suppressed the activity (with T_{50} values going up ~ 20 °C) of both pure Co and 1%Y-Co catalysts, probably due to the competition adsorption of H_2O with propane on the active sites or the shift of reaction equilibrium [55]. However, for 5%Y-Co, the light-off curves crossed before and after water addition; namely, in the presence of water, the low-temperature catalytic performance of 5%Y-Co was inhibited whereas the high-temperature one was promoted. When 5 vol.% H_2O was removed from the feed stream, the activity of 1%Y-Co was almost completely restored. The result demonstrated that 1%Y-Co was still highly active for propane oxidation (T_{90} = 265 °C) even under humid conditions.

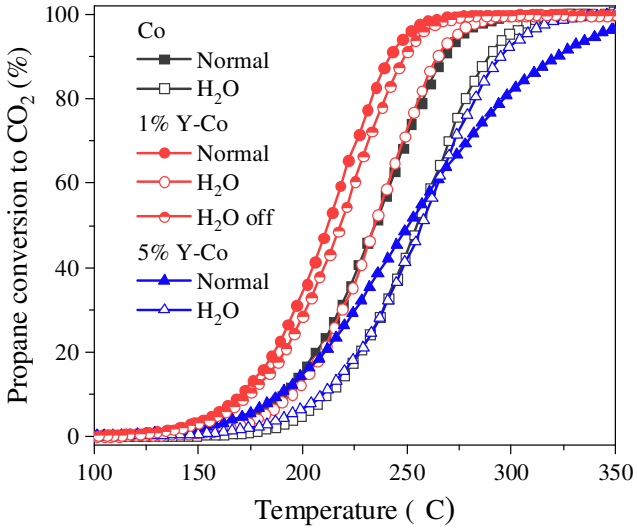

448

449 **Fig. 10.** Effect of 5 vol.% H_2O on the light-off curves of the catalysts in propane

450 oxidation (reaction conditions: toluene/propane concentration = 1000 ppm, O_2

451 concentration = 21 vol.% and WHSV = 40,000 mL g^{-1} h^{-1}).

452 **3.6. Discussion**

453 In this study, Y-Co oxides prepared from citrate sol-gel exhibited better catalytic

454 activity for toluene or propane combustion than pure Co oxide. The activity of the

455 Y-Co oxides was dependent on the atomic ratio of Y/(Co+Y), 1%Y-Co being the

456 most active catalyst. XRD, FTIR, Raman and N_2 adsorption analysis showed that low

457 content of Y (≤1%) can be randomly dispersed throughout the Co_3O_4 crystallite with

458 the formation of lattice defects and oxygen vacancies, while excess Y aggregates on

459 the surface of Co_3O_4 and forms Y carbonate species. The incorporation of Y can

460 restrain the growth of Co_3O_4 crystallites, resulting in smaller grains and larger surface

461 areas. H_2-TPR results evidenced that the low-temperature reducibility of the Y-Co

462 oxides increases until Y reaches 1%, then it decreases. TG-OSC revealed that Y

addition not only increased the number of surface oxygen species but also improved lattice oxygen mobility. XPS analysis demonstrated the presence of ample surface oxygen vacancies and adsorbed oxygen species in 1%Y-Co.

To get insight into the participation of oxygen species in the propane oxidation reaction, the catalytic test was performed from 50 to 450 °C over the catalysts in He flow. As shown in **Fig. S11**, free of gaseous O_2 supplying, only a small amount of CO_2 was produced below 350 °C, which should be originated from the consumption of surface oxygen species. In line with the TG-OSC analysis, more surface oxygen species were present in Y-Co catalysts than in pure Co catalyst. In 350–450 °C, abundant CO_2 occurred, signifying the participation of surface or bulk lattice oxygen in the reaction via a redox mechanism [10]. The CO_2 production at 450 °C over different catalysts follows the order: 1%Y-Co > 0.5%Y-Co > 0.25%Y-Co ≈ 3%Y-Co > Co > 5%Y-Co, which is consistent with their catalytic activity for propane oxidation under oxidation conditions. The result further revealed that more active oxygen species present in 1%Y-Co than in pure Co and other Y-Co catalysts. Considering the well-accepted redox mechanism for toluene or propane oxidation over Co_3O_4 catalysts, the superior catalytic performance of 1%Y-Co was correlated with the excellent reducibility and abundant reactive oxygen species that are able to participate in toluene or propane oxidation. Given the low activity of pure Y oxide, Y_2O_3 clusters aggregating on the surface of catalysts 3%Y-Co and 5%Y-Co may

block the active sites, which would explain their inferior activity for toluene or propane combustion.

4. Conclusion

Summarizing up, Y-modified Co_3O_4 catalysts with low contents of Y (0.25−5%), synthesized via citrate sol-gel, exhibited high efficiency for the total oxidation of toluene and propane. The optimal atomic ratio of Y/(Co+Y) was found to be 1%, with T_{90} values of 268 and 242 °C for toluene and propane oxidation, respectively, much lower than those of pure cobalt oxide (291 and 269 °C). In addition, catalyst 1%Y-Co demonstrated good cycling stability and long-term durability in propane oxidation. Appropriate incorporation of Y into Co_3O_4 greatly lowered the crystallite size, increased the surface area, promoted reducibility, and increased the number of surface oxygen species of the Y-Co catalysts. Excess Y will accumulate on the catalyst surface to form yttrium carbonate species, inhibiting the activity of the catalyst. The excellent performance of catalyst 1%Y-Co was attributed to its superior low-temperature reducibility and sufficient active oxygen species. This study provides a new point of view about designing an inexpensive and efficient catalyst for hydrocarbons elimination by introducing an appropriate amount of Y.

Acknowledgments

This work was financially supported by University Claude Bernard Lyon 1 and CNRS. We gratefully acknowledge the China Scholarship Council of P.R. China for ZHANG Weidong's grant. Special thanks to Dr. Alberto Rodríguez Gómez who performed the H_2-TPR experiments at Faculty of Chemical Science and Technology, University of Castilla-La Mancha.

References

[1] Y. Guo, M. Wen, G. Li, T. An, Recent advances in VOC elimination by catalytic oxidation technology onto various nanoparticles catalysts: a critical review, Appl. Catal. B Environ. 281 (2021) 119447. doi:10.1016/j.apcatb.2020.119447.

[2] S. Zhang, S. Liu, X. Zhu, Y. Yang, W. Hu, H. Zhao, R. Qu, C. Zheng, X. Gao, Low temperature catalytic oxidation of propane over cobalt-cerium spinel oxides catalysts, Appl. Surf. Sci. 479 (2019) 1132–1140. doi:10.1016/j.apsusc.2019.02.118.

[3] C. He, J. Cheng, X. Zhang, M. Douthwaite, S. Pattisson, Z. Hao, Recent Advances in the Catalytic Oxidation of Volatile Organic Compounds: A Review Based on Pollutant Sorts and Sources, Chem. Rev. 119 (2019) 4471–4568. doi:10.1021/acs.chemrev.8b00408.

[4] J. Chen, X. Chen, X. Chen, W. Xu, Z. Xu, H. Jia, J. Chen, Homogeneous introduction of CeOy into MnOx-based catalyst for oxidation of aromatic VOCs, Appl. Catal. B Environ. 224 (2018) 825–835. doi:10.1016/j.apcatb.2017.11.036.

[5] H. Zhang, X. Zheng, T. Xu, P. Zhang, Atomically Dispersed Y or La on Birnessite-Type MnO2 for the Catalytic Decomposition of Low-Concentration

524 Toluene at Room Temperature, ACS Appl. Mater. Interfaces. 13 (2021) 17532–
525 17542. doi:10.1021/acsami.1c01433.

526 [6] Z. Zhu, G. Lu, Y. Guo, Y. Guo, Z. Zhang, Y. Wang, X.Q. Gong, High
527 performance and stability of the Pt-W/ZSM-5 catalyst for the total oxidation of
528 propane: The role of tungsten, ChemCatChem. 5 (2013) 2495–2503.
529 doi:10.1002/cctc.201300101.

530 [7] Y. Luo, Y. Zheng, X. Feng, D. Lin, Q. Qian, X. Wang, Y. Zhang, Q. Chen, X.
531 Zhang, Controllable P Doping of the LaCoO3 Catalyst for Efficient Propane
532 Oxidation: Optimized Surface Co Distribution and Enhanced Oxygen Vacancies,
533 ACS Appl. Mater. Interfaces. 12 (2020) 23789–23799. doi:10.1021/acsami.0c01599.

534 [8] X. Li, X. Li, X. Zeng, T. Zhu, Correlation between the physicochemical
535 properties and catalytic performances of micro/mesoporous CoCeOx mixed oxides for
536 propane combustion, Appl. Catal. A Gen. 572 (2019) 61–70.
537 doi:10.1016/j.apcata.2018.12.026.

538 [9] Y. Jian, M. Tian, C. He, J. Xiong, Z. Jiang, H. Jin, L. Zheng, R. Albilali, J.-W.
539 Shi, Efficient propane low-temperature destruction by Co3O4 crystal facets
540 engineering: Unveiling the decisive role of lattice and oxygen defects and surface
541 acid-base pairs, Appl. Catal. B Environ. 283 (2021) 119657.
542 doi:10.1016/j.apcatb.2020.119657.

543 [10]L. Schick, R. Sanchis, V. González-Alfaro, S. Agouram, J.M. López, L.
544 Torrente-Murciano, T. García, B. Solsona, Size-activity relationship of iridium
545 particles supported on silica for the total oxidation of volatile organic compounds
546 (VOCs), Chem. Eng. J. 366 (2019) 100–111. doi:10.1016/j.cej.2019.02.087.

547 [11]W. Tang, W. Xiao, S. Wang, Z. Ren, J. Ding, P.-X. Gao, Boosting catalytic
548 propane oxidation over PGM-free Co3O4 nanocrystal aggregates through chemical

549 leaching: A comparative study with Pt and Pd based catalysts, Appl. Catal. B Environ.
550 226 (2018) 585–595. doi:10.1016/j.apcatb.2017.12.075.

551 [12] L. Ma, Y. Geng, X. Chen, N. Yan, J. Li, J.W. Schwank, Reaction mechanism of
552 propane oxidation over Co3O4 nanorods as rivals of platinum catalysts, Chem. Eng. J.
553 402 (2020) 125911. doi:10.1016/j.cej.2020.125911.

554 [13] Y. Shen, J. Deng, S. Impeng, S. Li, T. Yan, J. Zhang, L. Shi, D. Zhang, Boosting
555 Toluene Combustion by Engineering Co–O Strength in Cobalt Oxide Catalysts,
556 Environ. Sci. Technol. 54 (2020) 10342–10350. doi:10.1021/acs.est.0c02680.

557 [14] Q. Ren, S. Mo, R. Peng, Z. Feng, M. Zhang, L. Chen, M. Fu, J. Wu, D. Ye,
558 Controllable synthesis of 3D hierarchical Co3O4 nanocatalysts with various
559 morphologies for the catalytic oxidation of toluene, J. Mater. Chem. A. 6 (2018) 498–
560 509. doi:10.1039/C7TA09149D.

561 [15] W. Liu, R. Liu, X. Zhang, Controllable synthesis of 3D hierarchical Co3O4
562 catalysts and their excellent catalytic performance for toluene combustion, Appl. Surf.
563 Sci. 507 (2020) 145174. doi:10.1016/j.apsusc.2019.145174.

564 [16] Y. Ma, L. Wang, J. Ma, H. Wang, C. Zhang, H. Deng, H. He, Investigation into
565 the Enhanced Catalytic Oxidation of o -Xylene over MOF-Derived Co3O4 with
566 Different Shapes: The Role of Surface Twofold-Coordinate Lattice Oxygen (O 2f),
567 ACS Catal. 11 (2021) 6614–6625. doi:10.1021/acscatal.1c01116.

568 [17] B. Bai, H. Arandiyan, J. Li, Comparison of the performance for oxidation of
569 formaldehyde on nano-Co3O4, 2D-Co3O4, and 3D-Co3O4 catalysts, Appl. Catal. B
570 Environ. 142–143 (2013) 677–683. doi:10.1016/j.apcatb.2013.05.056.

571 [18] G. Li, C. Zhang, Z. Wang, H. Huang, H. Peng, X. Li, Fabrication of mesoporous
572 Co3O4 oxides by acid treatment and their catalytic performances for toluene
573 oxidation, Appl. Catal. A Gen. 550 (2018) 67–76. doi:10.1016/j.apcata.2017.11.003.

[19] Z. Zhu, G. Lu, Z. Zhang, Y. Guo, Y. Guo, Y. Wang, Highly Active and Stable Co3O4/ZSM-5 Catalyst for Propane Oxidation: Effect of the Preparation Method, ACS Catal. 3 (2013) 1154–1164. doi:10.1021/cs400068v.

[20] W. Zhang, Y. Zhou, M. Shamzhy, S. Molitorisová, M. Opanasenko, A. Giroir-Fendler, Total Oxidation of Toluene and Propane over Supported Co3O4 Catalysts: Effect of Structure/Acidity of MWW Zeolite and Cobalt Loading, ACS Appl. Mater. Interfaces. 13 (2021) 15143–15158. doi:10.1021/acsami.0c21999.

[21] G. Li, N. Li, Y. Sun, Y. Qu, Z. Jiang, Z. Zhao, Z. Zhang, J. Cheng, Z. Hao, Efficient defect engineering in Co-Mn binary oxides for low-temperature propane oxidation, Appl. Catal. B Environ. 282 (2021) 119512. doi:10.1016/j.apcatb.2020.119512.

[22] Z. Pu, Y. Liu, H. Zhou, W. Huang, Y. Zheng, X. Li, Catalytic combustion of lean methane at low temperature over ZrO2-modified Co3O4 catalysts, Appl. Surf. Sci. 422 (2017) 85–93. doi:10.1016/j.apsusc.2017.05.231.

[23] K. Wang, B. Liu, Y. Cao, Y. Li, D. Jia, V-modified Co3O4 nanorods with superior catalytic activity and thermostability for CO oxidation, CrystEngComm. 20 (2018) 5191–5199. doi:10.1039/C8CE00759D.

[24] M. Zhou, L. Cai, M. Bajdich, M. García-Melchor, H. Li, J. He, J. Wilcox, W. Wu, A. Vojvodic, X. Zheng, Enhancing Catalytic CO Oxidation over Co3O4 Nanowires by Substituting Co2+ with Cu2+, ACS Catal. 5 (2015) 4485–4491. doi:10.1021/acscatal.5b00488.

[25] J. Bae, D. Shin, H. Jeong, B.-S. Kim, J.W. Han, H. Lee, Highly Water-Resistant La-Doped Co3O4 Catalyst for CO Oxidation, ACS Catal. 9 (2019) 10093–10100. doi:10.1021/acscatal.9b02920.

598 [26] B. Feng, M. Shi, J. Liu, X. Han, Z. Lan, H. Gu, X. Wang, H. Sun, Q. Zhang, H.
599 Li, Y. Wang, H. Li, An efficient defect engineering strategy to enhance catalytic
600 performances of Co3O4 nanorods for CO oxidation, J. Hazard. Mater. 394 (2020)
601 122540. doi:10.1016/j.jhazmat.2020.122540.

602 [27] T. Baidya, T. Murayama, P. Bera, O. V. Safonova, P. Steiger, N.K. Katiyar, K.
603 Biswas, M. Haruta, Low-Temperature CO Oxidation over Combustion Made Fe- and
604 Cr-Doped Co3O4 Catalysts: Role of Dopant's Nature toward Achieving Superior
605 Catalytic Activity and Stability, J. Phys. Chem. C. 121 (2017) 15256–15265.
606 doi:10.1021/acs.jpcc.7b04348.

607 [28] J. Bae, D. Shin, H. Jeong, C. Choe, Y. Choi, J.W. Han, H. Lee, Facet-Dependent
608 Mn Doping on Shaped Co3O4 Crystals for Catalytic Oxidation, ACS Catal. 11 (2021)
609 11066–11074. doi:10.1021/acscatal.1c01666.

610 [29] G. Chai, W. Zhang, L.F. Liotta, M. Li, Y. Guo, A. Giroir-Fendler, Total oxidation
611 of propane over Co3O4-based catalysts: Elucidating the influence of Zr dopant, Appl.
612 Catal. B Environ. 298 (2021) 120606. doi:10.1016/j.apcatb.2021.120606.

613 [30] B. Martha, V.J. M., G.R. J., Synthesis of Highly Porous Yttria-Stabilized
614 Zirconia by Tape-Casting Methods, J. Am. Ceram. Soc. 86 (2004) 395–400.
615 doi:10.1111/j.1151-2916.2003.tb03311.x.

616 [31] M. Labaki, S. Siffert, J.-F. Lamonier, E.A. Zhilinskaya, A. Aboukaïs, Total
617 oxidation of propene and toluene in the presence of zirconia doped by copper and
618 yttrium, Appl. Catal. B Environ. 43 (2003) 261–271.
619 doi:10.1016/S0926-3373(02)00312-0.

620 [32] Z. Yang, N. Zhang, Y. Cao, M. Gong, M. Zhao, Y. Chen, Effect of yttria in
621 Pt/TiO2 on sulfur resistance diesel oxidation catalysts: Enhancement of
622 low-temperature activity and stability, Catal. Sci. Technol. 4 (2014) 3032–3043.
623 doi:10.1039/c4cy00424h.

[33] J. Yang, R. Wang, L. Yang, J. Lang, M. Wei, M. Gao, X. Liu, J. Cao, X. Li, N. Yang, Tunable deep-level emission in ZnO nanoparticles via yttrium doping, J. Alloys Compd. 509 (2011) 3606–3612. doi:10.1016/j.jallcom.2010.12.102.

[34] Y. Lou, J. Ma, X. Cao, L. Wang, Q. Dai, Z. Zhao, Y. Cai, W. Zhan, Y.Y. Guo, P. Hu, G. Lu, Y.Y. Guo, Promoting Effects of In2O3 on Co3O4 for CO Oxidation: Tuning O2 Activation and CO Adsorption Strength Simultaneously, ACS Catal. 4 (2014) 4143–4152. doi:10.1021/cs501049r.

[35] Y. Wang, K. Zheng, X. Hu, W. Zhou, X. Wei, Y. Zhao, Y2O3 promoted Co3O4 catalyst for catalytic decomposition of N2O, Mol. Catal. 470 (2019) 104–111. doi:10.1016/j.mcat.2019.04.002.

[36] T. Zhao, Y. Li, Q. Gao, Z. Liu, X. Xu, Potassium promoted Y2O3-Co3O4 catalysts for N2O decomposition, Catal. Commun. 137 (2020) 105948. doi:10.1016/j.catcom.2020.105948.

[37] L. Shi, Y. Jin, C. Xing, C. Zeng, T. Kawabata, K. Imai, K. Matsuda, Y. Tan, N. Tsubaki, Studies on surface impregnation combustion method to prepare supported Co/SiO2 catalysts and its application for Fischer-Tropsch synthesis, Appl. Catal. A Gen. 435–436 (2012) 217–224. doi:10.1016/j.apcata.2012.06.007.

[38] K. Nakamoto, Infrared and Raman Spectra of Inorganic and Coordination Compounds Part B: Applications in Coordination, Organometallic,and Bioinorganic Chemistry, 6th editio, John Wiley & Sons, New York, 2009.

[39] J. Xu, F. Huo, Y. Zhao, Y. Liu, Q. Yang, Y. Cheng, S. Min, Z. Jin, Z. Xiang, In-situ La doped Co3O4 as highly efficient photocatalyst for solar hydrogen generation, Int. J. Hydrogen Energy. 43 (2018) 8674–8682. doi:10.1016/j.ijhydene.2018.03.126.

[40] Y. Feng, L. Li, S. Niu, Y. Qu, Q. Zhang, Y. Li, W. Zhao, H. Li, J. Shi, Controlled synthesis of highly active mesoporous Co3O4 polycrystals for low temperature CO oxidation, Appl. Catal. B Environ. 111–112 (2012) 461–466. doi:10.1016/j.apcatb.2011.10.035.

[41] H. Guo, W. Zhang, L. Lou, A. Brioude, J. Mugnier, Structure and optical properties of rare earth doped Y2O3 waveguide films derived by sol-gel process, Thin Solid Films. 458 (2004) 274–280. doi:10.1016/j.tsf.2003.12.059.

[42] Y. Zhang, M. Gao, K. Han, Z. Fang, X. Yin, Z. Xu, Synthesis, characterization and formation mechanism of dumbbell-like YOHCO3 and rod-like Y2(CO3)3·2.5H2O, J. Alloys Compd. 474 (2009) 598–604. doi:10.1016/j.jallcom.2008.07.007.

[43] J. González-Prior, R. López-Fonseca, J.I. Gutiérrez-Ortiz, B. de Rivas, Oxidation of 1,2-dichloroethane over nanocube-shaped Co3O4 catalysts, Appl. Catal. B Environ. 199 (2016) 384–393. doi:10.1016/j.apcatb.2016.06.046.

[44] S. Mo, Q. Zhang, Y. Sun, M. Zhang, J. Li, Q. Ren, M. Fu, J. Wu, L. Chen, D. Ye, Gaseous CO and toluene co-oxidation over monolithic core-shell Co3O4-based hetero-structured catalysts, J. Mater. Chem. A. 7 (2019) 16197–16210. doi:10.1039/c9ta03750k.

[45] L. Li, Q. Yang, C. Zhang, J. Yan, Y. Peng, J. Li, Hollow-Structural Ag/Co3O4 Nanocatalyst for CO Oxidation: Interfacial Synergistic Effect, ACS Appl. Nano Mater. 2 (2019) 3480–3489. doi:10.1021/acsanm.9b00466.

[46] H. Liu, W. Jia, X. Yu, X. Tang, X. Zeng, Y. Sun, T. Lei, H. Fang, T. Li, L. Lin, Vitamin C-Assisted Synthesized Mn–Co Oxides with Improved Oxygen Vacancy Concentration: Boosting Lattice Oxygen Activity for the Air-Oxidation of 5-(Hydroxymethyl)furfural, ACS Catal. 11 (2021) 7828–7844. doi:10.1021/acscatal.0c04503.

[47] G. Chen, Y. Cai, H. Zhang, D. Hong, S. Shao, C. Tu, Y. Chen, F. Wang, B. Chen, Y. Bai, X. Wang, Q. Dai, Pt and Mo Co-Decorated MnO2 Nanorods with Superior Resistance to H2O, Sintering, and HCl for Catalytic Oxidation of Chlorobenzene, Environ. Sci. Technol. 55 (2021) 14204–14214. doi:10.1021/acs.est.1c05086.

[48] Z. Ren, Z. Wu, W. Song, W. Xiao, Y. Guo, J. Ding, S.L. Suib, P.-X. Gao, Low temperature propane oxidation over Co3O4 based nano-array catalysts: Ni dopant effect, reaction mechanism and structural stability, Appl. Catal. B Environ. 180 (2016) 150–160. doi:10.1016/j.apcatb.2015.04.021.

[49] W. Song, A.S. Poyraz, Y. Meng, Z. Ren, S.-Y. Chen, S.L. Suib, Mesoporous Co3O4 with Controlled Porosity: Inverse Micelle Synthesis and High-Performance Catalytic CO Oxidation at −60 °C, Chem. Mater. 26 (2014) 4629–4639. doi:10.1021/cm502106v.

[50] W. Yang, Y. Peng, Y. Wang, Y. Wang, H. Liu, Z. Su, W. Yang, J. Chen, W. Si, J. Li, Controllable redox-induced in-situ growth of MnO2 over Mn2O3 for toluene oxidation: Active heterostructure interfaces, Appl. Catal. B Environ. 278 (2020) 119279. doi:10.1016/j.apcatb.2020.119279.

[51] M. Han, X. Li, B. Li, N. Shi, K. Chen, J. Zhu, Z. Xu, Synthesis, characterization, and physicochemical properties of well-coupled Y2O3 nanobelt-Ag nanocrystals nanocomposites, J. Phys. Chem. C. 112 (2008) 17893–17898. doi:10.1021/jp806119w.

[52] E.M. Köck, M. Kogler, T. Bielz, B. Klötzer, S. Penner, In situ FT-IR spectroscopic study of CO2 and CO adsorption on Y2O3, ZrO2, and yttria-stabilized ZrO2, J. Phys. Chem. C. 117 (2013) 17666–17673. doi:10.1021/jp405625x.

[53] A. Bahgat Radwan, K. Ali, R.A. Shakoor, H. Mohammed, T. Alsalama, R. Kahraman, M.M. Yusuf, A.M. Abdullah, M. Fatima Montemor, M. Helal, Properties enhancement of Ni-P electrodeposited coatings by the incorporation of nanoscale

700 Y2O3 particles, Appl. Surf. Sci. 457 (2018) 956–967.
701 doi:10.1016/j.apsusc.2018.06.241.

702 [54]C. Wang, C. Zhang, W. Hua, Y. Guo, G. Lu, S. Gil, A. Giroir-Fendler, Catalytic
703 oxidation of vinyl chloride emissions over Co-Ce composite oxide catalysts, Chem.
704 Eng. J. 315 (2017) 392–402. doi:10.1016/j.cej.2017.01.007.

705 [55]W. Zhu, X. Chen, J. Jin, X. Di, C. Liang, Z. Liu, Insight into catalytic properties
706 of Co3O4-CeO2 binary oxides for propane total oxidation, Chinese J. Catal. 41
707 (2020) 679–690. doi:10.1016/S1872-2067(19)63523-0.

708 [56]W. Zhang, J. Díez-Ramírez, P. Anguita, C. Descorme, J.L. Valverde, A.
709 Giroir-Fendler, Nanocrystalline Co3O4 catalysts for toluene and propane oxidation:
710 Effect of the precipitation agent, Appl. Catal. B Environ. 273 (2020) 118894.
711 doi:10.1016/j.apcatb.2020.118894.

712

Y-modified Co_3O_4 catalysts for VOCs combustion